Bio-inspired Highly Scattering Networks via Polymer Phase Separation

Julia Syurik, Gianni Jacucci, Olimpia D. Onelli, Hendrik Hölscher, and Silvia Vignolini**

A common strategy to optimize whiteness in living organisms consists in using 3D random networks with dense and polydisperse scattering elements constituted by relatively low refractive index materials. Inspired by these natural architectures, a fast and scalable method to produce highly scattering porous polymer films via phase separation is developed. By varying the molecular weight of the polymer, the morphology of the porous films is modified, and therefore their scattering properties are tuned. The achieved transport mean free paths are in the micrometer range, improving the scattering strength of analogous low refractive index systems, e.g., standard white paper, by an order of magnitude. The produced porous films show a broadband reflectivity of ≈75% while only 4 µm thick. In addition, the films are flexible and can be readily index-matched with water (i.e., they become transparent when wet), allowing for various applications such as coatings with tunable transmittance and responsive paints.

1. Introduction

Colors in nature are often obtained by evolutionary-optimized complex nanoscale architectures.[1,2] This optimization is truly extraordinary if one considers the constraints that living organisms face in assembling these structures (i.e., the low refractive indexes of the starting materials, the need for mechanical stability as well as lightweight).[3] In the case of bright iridescent colorations, periodic architectures that are only few micrometers in thickness are capable of providing all these properties.[4] In contrast, obtaining an intense broadband reflection (i.e., white) in very thin layers is extremely challenging as the scattering

Dr. J. Syurik, Dr. H. Hölscher
Institute for Microstructure Technology
Karlsruhe Institute of Technology (KIT)
Hermann-von-Helmholtz-Platz 1
76344 Eggenstein-Leopoldshafen, Germany
E-mail: hendrik.hoelscher@kit.edu
G. Jacucci, O. D. Onelli, Dr. S. Vignolini
Department of Chemistry
University of Cambridge
Lensfield Road CB2 1EW, Cambridge, UK
E-mail: sv319@cam.ac.uk

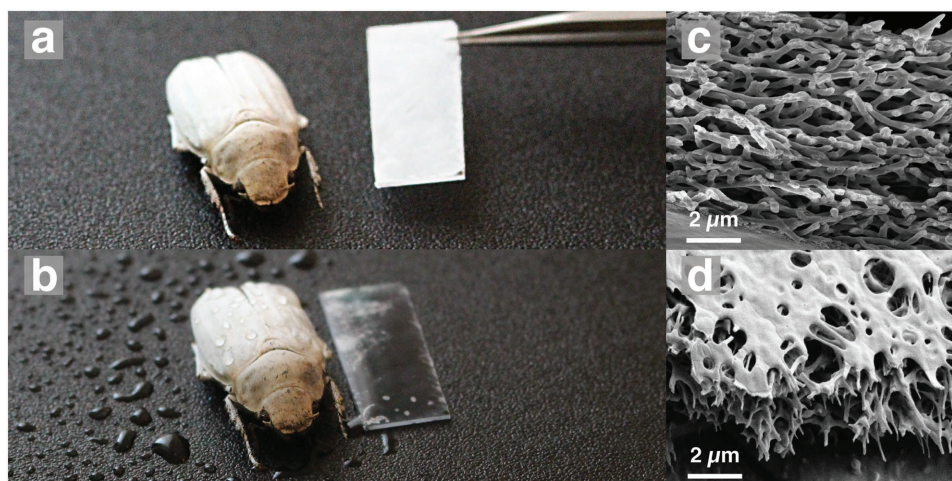The ORCID identification number(s) for the author(s) of this article can be found under https://doi.org/10.1002/adfm.201706901.

elements must be randomly arranged, typically decreasing the packing efficiency.[5–7] To compensate for the non-ideal packing, materials that are very highly scattering strength are generally chosen for industrial applications (i.e., materials with high refractive indexes).

A great example of multiple scattering optimization in a low refractive index medium is observed in the scales of *Cyphochilus* beetles (**Figure 1**a,c). Here, the anisotropic chitin network inside the scales which cover the insect's body outperforms all man-made low refractive index materials known to date.[3,8–11] The key to such optimization lies in the tuning of the filling fraction and in the anisotropic nature of the fibrillar structure in the scales.[3,10]

Inspired by these natural design principles, we fabricated highly scattering white networks solely constituted by polymethyl methacrylate (PMMA) (Figure 1b,d). The resulting porous films are flexible and show the shortest transport mean free path reported in the literature for low refractive index materials. We demonstrated that the scattering strength of the network can be enhanced by varying the molecular weight of PMMA to achieve transport mean free paths (l_t) as low as 1 µm for an incident wavelength around 500 nm. Having such a short transport mean free path yields a reflectance of 75% for a 4 µm thick film. Due to their low refractive index (close to 1.5 over the whole visible range) and porosity, the produced free-standing films can be easily index-matched with water and other conventional solvents, providing a tunable response, which transitions from white to transparent upon wetting (Figure 1b; Figure S1 and Movie S1, Supporting Information). This property, in addition with the high flexibility of the films (Figure S2 and Movie S2, Supporting Information), allows for various coating applications. We demonstrated that the scattering properties are maintained when the porous films are grinded into powders, opening their exploitation as white enhancers in paints, paper, and cosmetics.

2. Results and Discussion

The porous white films were obtained from PMMA by phase separation in solution (**Figure 2**a), a scalable process which is well known in the field of membrane technology.[12] In summary, we cast a three-component solution of PMMA (0.6 wt%) and water (<0.2 wt%) in acetone. After the rapid evaporation of acetone, the solution precipitated into two

**ADVANCED
SCIENCE NEWS**

www.advancedsciencenews.com

**ADVANCED
FUNCTIONAL
MATERIALS**

www.afm-journal.de

Figure 1. a) Similarly to the *Cyphochilus insulanus* beetle (left), microstructured PMMA films (right) exhibit a bright white appearance achieved by efficient multiple scattering. The film shown is 4 μm thick and is cast on a transparent PMMA substrate. b) Due to the pores on the surface, water can penetrate into the structure. Thus, the polymer film turns transparent when wet. The beetle does not change color upon wetting due to a continuous surface layer encasing the scales. A cross-sectional SEM image of a scale of a *Cyphochilus sp.* c) and of the PMMA film d) revealing the random networks that cause the bright white coloration by multiple light scattering.
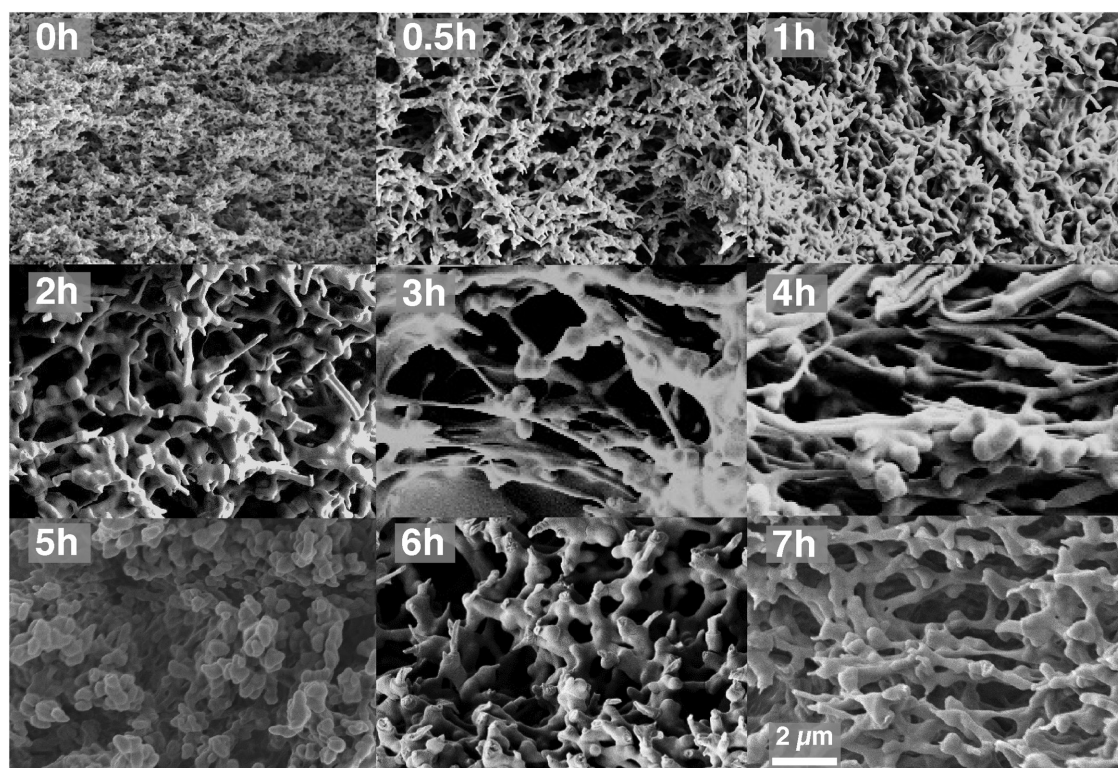
phases: a polymer-rich phase forming a random network and a liquid water phase, which evaporates at slower rate leading to the formation of nanoscale pores.

This simple assembly process strongly relies on the kinetics of the evaporation and hence on the composition of the solution. Only a small percent variation in the water content or in

the molecular weight and polydispersity (D) of the polymer chains greatly affects the assembly. Therefore, to control these parameters, PMMA with different number average molar mass (M_n) and mass average molar mass (M_w) were prepared via sonication treatment starting from commercial PMMA with initial $M_w = 1.86$ MDa. The values of M_n and M_w were
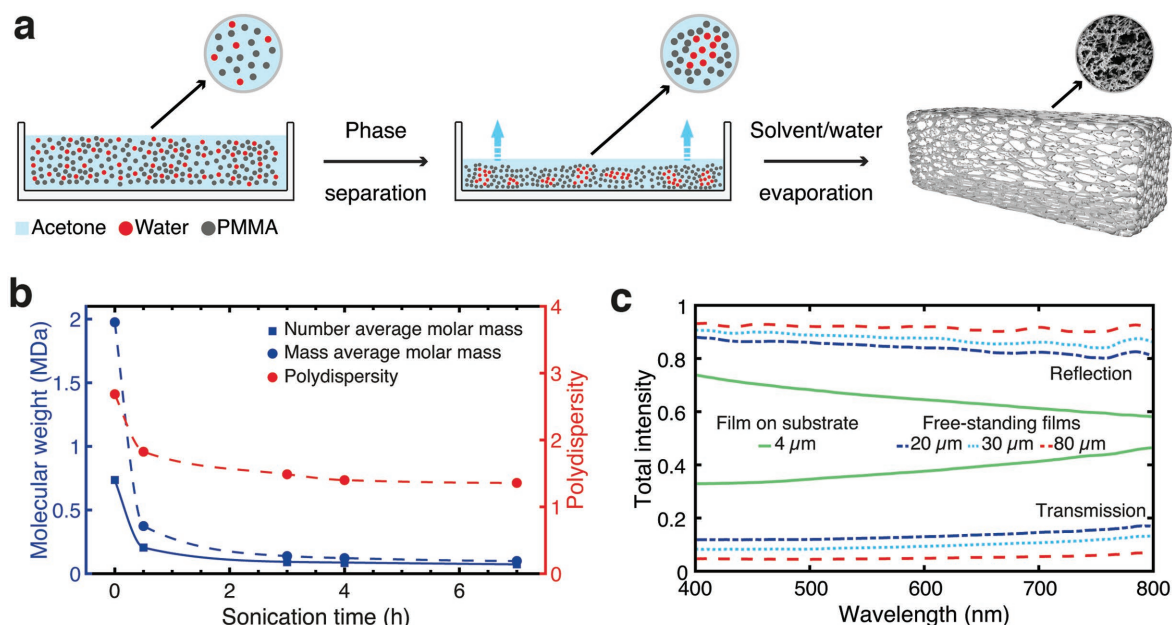
Figure 2. a) Fabrication route for the bioinspired white films. A three-component solution of PMMA (0.6 wt%) and water (<0.2 wt%) in acetone is cast under controlled environmental conditions and allowed to evaporate. The solution precipitates into two phases after the quick evaporation of the acetone: a polymer-rich phase forming the random network and a liquid water phase. Next, the water evaporates leading to the final porous polymer structure. The round insets show a magnification of the self-assembly steps and an SEM image of the polymer network. b) Values of number average molar mass and of mass average molar mass determined at different stages of sonication by SEC. Both quantities decrease with sonication duration. After 7 h of treatment, they are only 5% and 11% of the initial value, respectively. The polydispersity is roughly halved after 7 h of sonication. The lines connecting the data point are guides for the eye. c) Total transmission and total reflection for free-standing (20, 30, and 80 μm thick) and ultrathin (4 μm thick) PMMA films. The ultrathin 4 μm thick film is cast on a PMMA substrate (see Figure 1). The samples were cast after 3 h of sonication.

ADVANCED
SCIENCE NEWS
www.advancedsciencenews.com

ADVANCED
FUNCTIONAL
MATERIALS
www.afm-journal.de

Figure 3. Typical SEM images of the cross-section of porous films obtained by varying the sonication time between 0 and 7 h. The most scattering microstructures are observed for films sonicated from 1 to 3 h.

estimated at different stages of sonication using size exclusion chromatography (SEC). As expected, both M_n and M_w gradually decrease with the sonication time (Figure 2b).[13] Similarly, the polydispersity (D) of the films decreased from 2.7 for nonsonicated PMMA to 1.4 after 7 h of sonication.

After sonication, nine different acetone solutions containing 0.6 wt% of PMMA at different sonication stages (after 0.5, 1, 2, 3, 4, 5, 6, and 7 h) were used to cast films under identical conditions. The sonicated solutions were used to cast free-standing films (between 12 and 85 µm thick). In addition, ultrathin films (with a thickness ranging from 1.5 to 4.0 µm) were cast from the 3 h sonicated solution. Acetone is moderately hygroscopic,[14] and therefore can potentially attract water in the solution in linear dependence with the duration of the sonication. However, no significant difference in the water content for the nonsonicated and sonicated solutions was revealed via Fourier transform infrared (FTIR) spectroscopy, allowing to estimate the water content in all the solutions to be below 0.2 vol% (0.16 wt%) prior to casting (for details regarding the FTIR measurements refer to Figure S3, Supporting Information).

Figure 2c displays examples of total reflectivity and transmissivity spectra for free-standing films and for an ultrathin film cast after 3 h of sonication. The total transmission spectra related to the other sonication times and the specular reflection contribution with respect to the total reflectivity can be found in Figures S4 and S5 in the Supporting Information, respectively.

The scanning electron microscopy (SEM) images reported in **Figure 3** reveal the crucial effect of the sonication time on the morphology of the films. The films obtained from nonsonicated

PMMA solution showed a fibrillar network with very low porosity, whose PMMA filling fraction was determined from SEM images to be about 75% and with fibrils below 100 nm in length and 20 nm in width. An increase in the sonication time led to a rise in the porosity as well as to larger struts, both in length and width. From the SEM images, we can roughly estimate that, after 1 h of sonication, the length of the fibrils constituting the network ranged from 500 to 1200 nm in length and between 120 and 300 nm in thickness. In contrast, after 2 h, the average length has increased to about 2000 nm and the width was 400 nm. When extending the sonication time to 4 h, the struts became more elongated with a length of 3.5–4.5 µm and a thickness of about 300 nm. Lengthening the sonication time even further revealed an opposite trend: the fibrils become smaller and thicker. Finally, the film produced from PMMA sonicated for 7 h showed a similar morphology to the nonsonicated films, with a PMMA fraction of ≈65%. The change of morphology can be intuitively explained considering that PMMA forms a kinetically stable aqueous bi-phasic system which does not collapse upon complete evaporation of the solvents (i.e., leading to the desired porosity) only for specific values of viscosity, and therefore for a specific interval of molecular weights.

To characterize quantitatively the light transport of the films we estimated the transport mean free path (l_t) for different sonication stages. More in detail, we measured the total transmission in a series of films with the same morphology but different thickness. To evaluate l_t, we used the analytical expression, which correlates the total transmission (T) and the thickness (L) in the diffusion approximation for a slab geometry[5,6]

$$T = \frac{1}{L_a} \frac{\sinh\left(\frac{2z_e}{L_a}\right)\sinh\left(\frac{z_e}{L_a}\right)}{\sinh\left(\frac{L+2z_e}{L_a}\right)} \qquad (1)$$

where L_a is the absorption length and z_e is the extrapolation length. The latter considers the effect of internal reflections at the film surfaces in the evaluation of l_t.[15–17] The extrapolation length was determined from the angular distribution measurement of the transmitted light and found to be $z_e = (1.48 \pm 0.14) l_t$ (more details in Figure S6, Supporting Information).[18] This result is in good agreement with the values reported in the literature for analogous systems.[10,19]

As the absorption length, L_a, for PMMA is negligible (as confirmed also by the fact that the sum of total transmission and total reflection is close to 1 as shown in Figure 2c), Equation (1) can be simplified to

$$T \approx \frac{2z_e}{L+2z_e} \qquad (2)$$

The values of l_t obtained from fitting the transmission behavior as function of the thickness using Equation (2) are shown in **Figure 4**b. The data reported in Figure 4b are obtained for wavelengths around 500 nm. However, these are representative of the scattering behavior over the whole visible range as the spectral response of the transmission in function of the thickness has only a weak dispersion (the wavelength dependency of l_t is further investigated in Figure S7, Supporting Information). The l_t values of the films obtained after sonication times between 1 and 3 h are one order of magnitude smaller than that of commercial white paper.[9,19] Furthermore, the produced bioinspired films outperform the reported scattering strength for cellulose nanostructures and the *Cyphochilus sp.* beetle (green and blue lines in Figure 4b, respectively).[9,19]

The scattering properties of the films were further characterized measuring the angular distribution of the scattered light using a goniometer (Figure S8, Supporting Information). We observed that the light scattered from the films follows a Lambertian profile, implying that their bright white appearance does not depend on the observation angle. This property is very desirable for paints and other applications.

To further investigate how the morphology of the produced porous materials affects the scattering performance, a set of thinner films was prepared after 3 h of sonication. While for the films discussed above, the evaporation kinetics is similar across the whole set, in the case of very thin films, the self-assembly process occurs almost instantaneously due to the small volumes involved (≈0.2–1 mL). Therefore, even if we
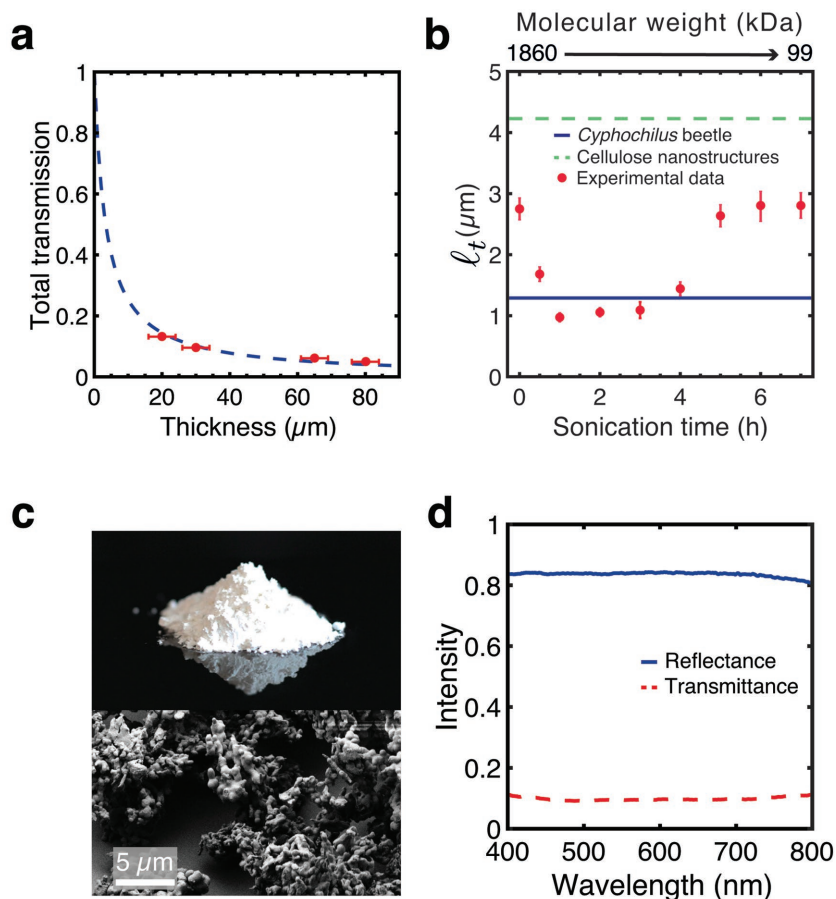
Figure 4. a) Total transmittance as a function of the film thickness after 3 h of sonication. The dotted lines represent the theoretical fit from which the mean free path (l_t) has been extrapolated. The error bars on the total transmission are smaller than the markers. b) l_t for films obtained after different sonication times (bottom axis), i.e., different molecular weights of the polymer (top axis). The error bars represent the confidence interval of the fit. l_t is estimated at 500 nm (wavelength of the impinging light). The l_t at 500 nm for the *Cyphochilus* beetle and the cellulose nanostructures are reported in refs. [9] and [19], respectively. c) A photograph of the powder obtained by milling the white PMMA film (upper panel) and an SEM image of the powder (lower panel) revealing that diameters of the particles do not exceed 20 μm, allowing the use of this material as white enhancers in paints, paper, and cosmetics. d) Total reflection and total transmission of the PMMA powder.

observed similar dimension of the struts with respect to the previous set of samples, we did not include them in the scattering mean free path measurements reported in Figure 4b. These ultrathin films not only maintain a Lambertian distribution for the scattered light (Figure S9, Supporting Information), but they also exhibit a high scattering efficiency. In fact, a 4 μm thick film obtained from a fast self-assembly kinetic reflects around 75% of the incident light (Figure 2c). Compared with the free-standing samples, which show an almost wavelength-independent reflectivity, the ultrathin samples have a higher reflectivity at short wavelengths. This spectral behavior, which can be explained as a thickness-related effect,[20] gives rise to an enhanced white perception to the human eye.[11]

Additional functionality can be achieved by milling the PMMA porous films into a powder whose particle sizes are below 20 μm. Although some morphological changes were

introduced during the milling process, the powder still revealed a rich microstructure.

The total reflectance spectra from the powder (Figure 4d) remain high and comparable to that of commercial titanium dioxide powders while using a material with almost the half of the refractive index and less than a third of the density.[21,22]

3. Conclusion

In conclusion, we have shown a simple and scalable route to fabricate highly scattering materials by optimizing the morphology of a low refractive index medium. The bio-inspired films obtained in this work reflect more than 75% in just a few micrometers of thickness while retaining two valuable features of PMMA: flexibility and lightweight. Moreover, using conventional liquids such as water or ethanol, it is possible to index-match the films providing a fully reversible change of appearance from white to transparent and vice versa. The combination of a scalable manufacturing technique with the optical functionality of the materials is extremely appealing for the application of these films as functional coatings. Finally, achieving a very short scattering mean free path is also important from a fundamental science point of view: a replica of such porous network using a higher refractive index material might allow the observation of strong localization phenomena.[23–26]

4. Experimental Section

Preparation of Porous PMMA Films: As-received PMMA sheets (Topacryl AG, $M_n = 0.64$ MDa, $M_w = 1.86$ MDa) were fully dissolved in acetone (EMSURE, water content < 0.05 wt%, Merck, Cas-Nr. 67-64-1) in concentration of 0.6 g/100 mL. Afterward, the solution was treated with a horn sonicator (Qsonica Q125, Qsonica) for a time interval between 30 min and 7 h, with the aim of tuning the length of the PMMA chains in solution and thus the microstructure of the final films. The sonication was performed in a closed chamber and the flask containing the PMMA–acetone solution was surrounded by icy water for cooling. Due to the nonnegligible water content in the solvent and the PMMA sheets (1%, as-received), the resulting solution was a classic three-component system constituted by a polymer (PMMA), a solvent (acetone), and nonsolvent (water).[12]

The solutions were cast in glass beakers with a diameter of 11 cm and left to rest for solvent evaporation and subsequent phase separation. When the solvent was fully evaporated, the porous microstructure of the film was solidified and therefore fixed. The duration of the drying step was about 10 min for a 20 mL solution. Films with the thicknesses in the range (15 ± 1) μm and (85 ± 3) μm were produced by casting different amounts of solutions. The environmental conditions were as follows: relative humidity $(31 \pm 7)\%$, temperature (21 ± 1) °C.

Morphological Analysis: The thickness of microstructured films (after peeling them off the glass support) at five positions for each sample was measured using an incremental measuring probe (MT60 M, Heidenhain) with a precision of ±0.5 μm. The average value was then calculated. The measured film thicknesses agreed with the values determined from SEM images of the films cross-sections as recorded using a SUPRA 60 VP SEM (Zeiss) with an accelerating voltage between 1.5 and 4 kV. Prior to SEM analysis, the samples were cooled down in liquid nitrogen and cracked. The surface of interest was sputter coated with 4 nm silver using a Sputter-Coater (K575X, Emitech) to avoid charging effects.

SEC: The number average molar mass (M_n), the mass average molar mass (M_w), and the polydispersity (D) for the untreated and foamed samples were determined via SEC. Here, an Agilent 1200 Series Gel Permeation and Size Exclusion Chromatography System (with a refractive index detector) equipped with columns from Polymer Standards Service GmbH (PSS SDV Lux 5m 1000 and 10^5 Å) was used. The measurements were performed at room temperature with a flow rate of 1 mL min^{-1} and the eluent was tetrahydrofuran. PMMA Standards from PSS Polymer Standards Service GmbH were used for calibration. Five cast porous films produced by sonication for 0, 0.5, 3, 4, and 7 h and one reference sample (as-received transparent PMMA) were analyzed.

Transport Mean Free Path Measurements: The transport mean free path (l_t) of the polymer films was determined using total transmission/reflectance measurements. A light source (Ocean Optics HPX-2000) was coupled into an optical fiber (Thorlabs FC-UV100-2-SR) via a collimator (Thorlabs). The emission spectrum of the light source limits the experimental range of wavelengths between 400 and 800 nm. The transmitted/reflected light was collected with an integrating sphere (Labsphere) and the signal was acquired by a spectrometer (Avantes HS2048). For total reflection measurements, the signal was normalized with respect to the coating of the integrating sphere. For the total transmission measurement, the signal was normalized with respect to the intensity when no sample was mounted. All measurements were recorded using unpolarized light and an integration time equal to 2 s. Five spectra were taken for each sample and averaged to reduce the signal-to-noise ratio.

Supporting Information

Supporting Information is available from the Wiley Online Library or from the corresponding author.

Conflict of Interest

The authors declare no conflict of interest.

Keywords

bio-inspired materials, functional coatings, polymeric-films, scattering, whiteness

[1] A. R. Parker, V. L. Welch, D. Driver, N. Martini, *Nature* **2003**, *426*, 786.

[2] P. Vukusic, in *Optical Interference Coatings*, (Ed.: N. Kaiser), Springer, Berlin, Germany **2003**, pp.1–34.

[3] B. D. Wilts, X. Sheng, M. Holler, A. Diaz, M. Guizar-Sicairos, J. Raabe, R. Hoppe, S.-H. Liu, R. Langford, O. D. Onelli, D. Chen, S. Torquato, U. Steiner, C. G. Schroer, S. Vignolini, A. Sepe, *Adv. Mater.* **2017**, 1702057.

[4] S. Kinoshita, S. Yoshioka, *Rep. Prog. Phys.* **2008**, *71*, 76401.

[5] D. S. Wiersma, *Nat. Photonics* **2013**, *7*, 188.

[6] A. Ishimaru, *Wave Propagation and Scattering in Random Media*, Academic, New York, NY **1989**.

[7] P. Sheng, *Introduction to Wave Scattering, Localization and Mesoscopic Phenomena*, Springer, Berlin, Germany **2006**.

[8] P. Vukusic, B. Hallam, J. Noyes, *Science* **2007**, *315*, 348.

[9] M. Burresi, L. Cortese, L. Pattelli, M. Kolle, P. Vukusic, D. S. Wiersma, U. Steiner, S. Vignolini, *Sci. Rep.* **2014**, *4*, 6075.

[10] L. Cortese, L. Pattelli, F. Utel, S. Vignolini, M. Burresi, D. S. Wiersma, *Adv. Opt. Mater.* **2015**, *3*, 1337.

[11] S. M. Luke, B. T. Hallam, P. Vukusic, *Appl. Opt.* **2010**, *49*, 4246.

[12] J. Mulder, *Basic Principles of Membrane Technology*, Springer Science & Business Media, Dordrecht, Netherlands **2012**.

[13] N. Daraboina, G. Madras, *Ultrason. Sonochem.* **2009**, *16*, 273.

[14] B. Tan, P. Melius, P. Ziegler, *J. Chromatogr. Sci.* **1982**, *20*, 213.

[15] A. Lagendijk, R. Vreeker, P. De Vries, *Phys. Lett. A* **1989**, *136*, 81.

[16] J. X. Zhu, D. J. Pine, D. A. Weitz, *Phys. Rev. A* **1991**, *44*, 3948.

[17] D. Contini, F. Martelli, G. Zaccanti, *Appl. Opt.* **1997**, *36*, 4587.

[18] M. U. Vera, P. A. Lemieux, D. J. Durian, *J. Opt. Soc. Am. A* **1997**, *14*, 2800.

[19] S. Caixeiro, M. Peruzzo, O. D. Onelli, S. Vignolini, R. Sapienza, *ACS Appl. Mater. Interfaces* **2017**, *9*, 7885.

[20] J. Syurik, R. H. Siddique, A. Dollmann, G. Gomard, M. Schneider, M. Worgull, G. Wiegand, H. Hölscher, *Sci. Rep.* **2017**, *7*, 46637.

[21] P. Mou, P. Umapada, J. M. Gracia, Y. Jiménez, F. Pérez-Rodríguez, *Nanoscale Res. Lett.* **2012**, *7*, 1.

[22] X. Chen, S. S. Mao, *Chem. Rev.* **2007**, *107*, 2891.

[23] P. W. Anderson, *Philos. Mag. B* **1985**, *52*, 505.

[24] Q. Gao, X. Wu, Y. Fan, *Dyes Pigm.* **2014**, *109*, 90.

[25] A. Lagendijk, B. van Tiggelen, D. S. Wiersma, *Phys. Today* **2009**, *62*, 24.

[26] S. E. Skipetrov, J. H. Page, *New J. Phys.* **2016**, *18*, 21001.